

Switchable triple band-notched UWB antenna modelling for interference rejection from dual WiMAX bands and satellite C-band service

Partha Pratim Shome & Taimoor Khan

To cite this article: Partha Pratim Shome & Taimoor Khan (2020): Switchable triple band-notched UWB antenna modelling for interference rejection from dual WiMAX bands and satellite C-band service, *Journal of Electromagnetic Waves and Applications*, DOI: [10.1080/09205071.2020.1806115](https://doi.org/10.1080/09205071.2020.1806115)

To link to this article: <https://doi.org/10.1080/09205071.2020.1806115>



Published online: 17 Aug 2020.



Submit your article to this journal 



Article views: 10

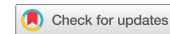


View related articles 



CrossMark

View Crossmark data 



Switchable triple band-notched UWB antenna modelling for interference rejection from dual WiMAX bands and satellite C-band service

Partha Pratim Shome and Taimoor Khan

Department of Electronics and Communication Engineering, National Institute of Technology, Silchar, India

ABSTRACT

A triple band-notched monopole antenna with reconfigurable characteristics is designed and investigated in this study for implementation in ultra-wideband (UWB) systems. A conventional rectangular monopole antenna is intended first to accomplish UWB performance characteristics. Further, to obtain triple notched characteristics, three U-shaped slots are etched on the rectangular radiating surface of the antenna. A wide frequency bandwidth ranging from 2.13 GHz to 10.50 GHz with three notched bands operating at 2.65 GHz (2.49–2.82 GHz), 3.43 GHz (3.18–3.68 GHz), and 4.08 GHz (3.93–4.22 GHz) have been successfully realized. By integrating three PIN diode switches, total eight reconfigurable states of operations have been realized in the UWB spectrum. A thorough analytical investigation along with the comparison of simulated and measured performances for the proposed antenna has been presented to manifest the applicability in practical systems. The antenna structure can be successfully implemented for rejecting interferences from dual WiMAX bands along with C-band fixed satellite communication systems, respectively.

ARTICLE HISTORY

Received 15 January 2020

Accepted 1 August 2020

KEYWORDS

Reconfigurable antenna;
triple notch; PIN diode;
equivalent circuit modelling;
U-slot; ultra-wideband

1. Introduction

With rapid advancements in wireless technologies, multiple applications have emerged out for implementation in practical systems. Among all these technologies, UWB system has gained maximum attention among the researchers because of its advantages such as low power consumption, short-range communications with the high data rate, etc. [1]. As a front-end component in UWB systems, antenna plays an important role in controlling the efficiency of the overall system. The UWB antennas are desired to operate over the frequency range from 3.1 to 10.6 GHz specified by the Federal Communications Commission (FCC) and exhibit stable radiation characteristics over this complete frequency spectrum [2]. However, one of the key challenges encountered in implementing UWB systems is the increasing interferences from different narrowband radio applications. The part of spectrum specified for the UWB technology share with some narrowband

technologies, such as WLAN (2.4–2.484 GHz/5.15–5.35 GHz/5.725–5.825 GHz), WiMAX (2.5–2.69 GHz/3.4–3.69 GHz/5.25–5.825 GHz), C-band (3.7–4.2 GHz/5.925–6.425 GHz) and X-band (7.25–7.75 GHz/7.9–8.4 GHz). Thus, the spectrum sharing scenario causes electromagnetic interference with the UWB system and degrades its performance [3].

In order to overcome the limitations of unwanted potential interferences, band notch characteristics in UWB antennas have been introduced. The traditional approach to overcome this problem is to add a narrowband band-stop filter (BSF) at the end of the antenna. However, this approach increases the design complexity and system cost as well [4]. Different alternatives are therefore investigated for introducing band rejection features in UWB antennas. To find notched behaviour in the UWB range, various techniques have been used such as embedding quarter- or half-wavelength slots [5–7], quarter-wavelength stubs [8], EBG structures [9], parasitic resonating structures [10,11], etc. With the help of these techniques, several researchers have designed single band-notched [12,13], dual band-notched [14,15], triple band-notched [16,17], quadruple band-notched [18,19], and quintuple band-notched [20,21] UWB antennas in last decade to reject interferences from multiple narrowband systems. But these designs permanently reject the notch-bands once it is fabricated. However, sometimes band rejection is not necessary when there is no co-existence with narrowband systems. In this scenario, antenna structure should be able to transform in such a way that it leads to reconfigure a stopband into passband. To overcome this limitation, smart self-adaptable UWB antennas are desired having the capability to reconfigure its notched behaviour as per the system requirement. Recently, these self-adaptable antenna systems are extensively preferred for cognitive radio (CR) applications.

In order to ensure dynamical performance characteristics, antennas are employed with different switches such as mechanical actuators, phase shifters, MEMS switches, PIN diodes, or varactor diodes [22]. In recent years, antenna engineers have paid their extensive attention in developing novel structures to achieve reconfigurable characteristics electronically in UWB antennas [23–30]. Valizade et al. [23] have designed a square slot antenna embedded with Π -shaped slot on the radiating stub for generating band-notched characteristics. Further, by utilizing a PIN diode across the Π -shaped slot reconfigurable band-notched characteristics have been obtained for switching the operating state between different modes and rejecting interferences from existing wireless systems. Yadav et al. [24] have realized a frequency reconfigurable antenna with switchable functionality between 5.3 GHz notched-band UWB antenna to 5.3 GHz WLAN antenna. An F-shape parasitic element with three stubs connected and disconnected with metallic ground plane is implemented using PIN diodes to form the reconfigurable structure. A compact monopole antenna using G-shaped radiator is designed first and then embedded with a PIN diode between the poles of G-shaped radiator to develop reconfigurable characteristics for successfully rejecting interferences from WiMAX and C-band satellite systems in [25]. Badamchi et al. [26] have etched two U-shaped slots with folded arms on the radiating plane and then embedded two PIN diodes along these slots to add switchable single and dual band notch performances. Similarly, a circular slot antenna has been perceived in [27] where the radiating element has been included with a semi-circular parasitic strip and a T-shaped stub for realizing dual band-notched characteristics. Next by connecting the parasitic strip and loaded stub with PIN diodes and then configuring the diodes in prescribed combination the reconfigurable capability is achieved. By utilizing PIN diodes, Nasrabadi et al. [28] have

designed reconfigurable triple band-notched antenna with the capability to operate in five different states. A single/dual-band notched reconfigurable antenna is demonstrated in [29] using two PIN diodes for efficient utilization of UWB spectrum in case of no interference scenario. Off late, Nazeri et al. [30] have investigated a fractal UWB antenna with triple band-notched characteristics and then realized reconfigurability by attaching PIN diodes to appropriate slot structures. It has been observed that, to meet the requirement of achieving better spectrum utilization in CR systems, antennas are desired to be capable of operating in multiple states. In general, more number of operating states can improve the efficiency and usefulness of an antenna for practical CR environment which are usually achieved by employing multiple switching elements. However, incorporation of multiple switching elements and its associated biasing circuit contributes in producing additional losses, larger circuit area and increasing design complexity. Designing appropriate biasing circuit to turn ON/OFF the switching element, therefore, holds a great challenge. In the open literature, many advanced UWB antennas with reconfigurable band-notched characteristics have been studied, however, mostly for single/dual-notched configurations which can be operated for maximum up to four different operating states. Further, the reported articles have also failed to achieve all the possible operational modes given the number of rejected bands. Till date, limited research on triple-notched UWB antenna with reconfigurable capability is performed. Besides, the review study conducted in [31] reveals that most of the existing UWB antenna configurations, available in the open literature, are targeted for rejecting interference from WiMAX and WLAN only. With the increasing popularity of wireless systems, several other applications have been proposed which also share the spectrum or possess interference threats to the existing UWB band. In this paper, a rectangular printed monopole UWB antenna with triple notched-band configurations to filter out interferences from dual WiMAX bands (2.49–2.82 GHz, 3.18–3.68 GHz), and C-band satellite communication systems (3.93–4.22 GHz), is presented and fabricated. By employing three U-shaped slots, the notched characteristics have been obtained. Reconfigurability is then introduced in the antenna structure to enhance operating flexibility. The performance analysis of the antenna structure is conducted with the help of commercially available ANSOFT HFSS simulator. The optimized configuration of the proposed design has an overall dimension of $34.9 \times 31.3 \times 1.6 \text{ mm}^3$.

2. Proposed antenna configuration

In this section, geometrical configuration of the proposed antenna with the design process has been discussed. In the first step of the design procedure, a traditional rectangular printed monopole antenna is conceptualized as the reference UWB antenna design (Figure 1(a)). This reference design contains a rectangular-shaped radiator on a dielectric substrate fed by a 50Ω microstrip line. A partial ground plane structure is designed on the other side of the substrate in order to achieve impedance matching over a wide frequency range. FR4 material (dielectric constant = 4.4, thickness = 1.6 mm and loss tangent = 0.02) is used as dielectric substrate. In order to introduce notched characteristics, three U-shaped slots are then incorporated on the radiating surface. Slot #1 (outer U-shaped slot) is incorporated to obtain the first notch at 2.69 GHz. Similarly, Slot #2 (middle U-shaped slot) and Slot #3 (inner U-shaped slot) are etched to produce second and third notches at

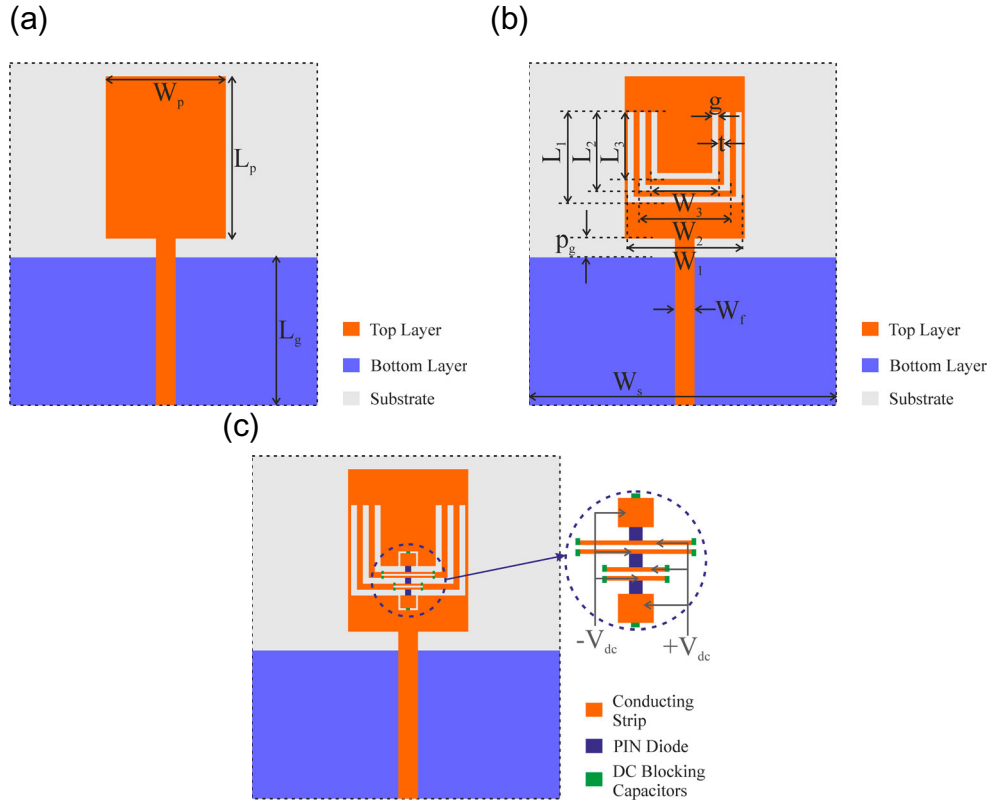


Figure 1. (a) Geometrical layout of reference UWB antenna configuration. (b) Geometrical layout of proposed notched antenna configuration. (c). Geometrical layout of proposed reconfigurable antenna configuration.

3.31 and 4.15 GHz, respectively. Figure 1(b) shows the optimized geometric layout of the proposed triple-notched design.

Initial estimation of the geometrical parameters of the reference UWB monopole antenna was done based on empirical relation defined using Equations (1)–(2), respectively [32]:

$$f_L = \frac{7.2}{(L_p + W_p/2\pi + p_g) \times k} \text{GHz} \quad (1)$$

Here,

f_L = Lower cut-off frequency (GHz)

L_p = Length of the rectangular monopole (cm)

W_p = Width of the rectangular monopole (cm)

p_g = Feed gap (cm)

The factor k is taken into consideration of the effect of dielectric material on to the performance of lower band edge frequency and can be approximately taken as:

$$k = \sqrt{\epsilon_{eff}} \quad (2)$$

Similarly, the estimation of the dimension of the three U-shaped slots is done based on Equations (3)–(5), respectively [33]. By varying the length of the U-shaped slots, the notch frequency can be properly adjusted:

$$f_n^i = \frac{c_0}{2L_{slot}^i \sqrt{\epsilon_{eff}}} \quad (3)$$

$$L_{slot}^i = 2L_i + W_i \quad (4)$$

$$\epsilon_{eff} \approx \frac{\epsilon_r + 1}{2} \quad (5)$$

Here, c_0 is speed of light in free space (3×10^8 m/sec), f_n^i is i^{th} notch frequency, (where $i = 1, 2$ and 3 for Slot #1, Slot #2 and Slot #3), and ϵ_{eff} is the effective dielectric constant.

Based on the initial approximated geometrical parameters, the antenna, presented in Figure 1(a), is designed using HFSS v14.0 software. Through simulation, further optimization of the geometrical parameters is performed to achieve the desired performance characteristics. The optimized dimensions of the triple-notched antenna configuration are obtained as: $L_s = 34.9$, $W_s = 31.3$, $L_p = 16.5$, $W_p = 12.2$, $L_1 = 9.2$, $L_2 = 8$, $L_3 = 6.8$, $W_1 = 11.6$, $W_2 = 9.2$, $W_3 = 6.8$, $L_g = 15.1$, $W_f = 2.0$, $t = 0.6$, $g = 0.6$. Here all dimensions are in mm.

After designing the triple notched UWB antenna, reconfigurable characteristic is then introduced to switch the notched frequencies between different operating states. To meet this objective, three PIN diodes are utilized in order to reconfigure these notches. Surface mountable low loss SMP1345-040LF PIN diodes from Skyworks Solutions have been utilized to achieve the desired reconfigurable characteristics. Figure 1(c) shows the proposed reconfigurable triple notched UWB antenna together with the biasing circuit. The biasing circuit is a combination of PIN diode sandwiched between two DC blocking capacitors of 10 pF each. The blocking capacitors are used to avoid the DC signal from interfering with RF input. The equivalent circuit for PIN diode under ON and OFF states of operations are described in Figure 2(a), and Figure 2(b), respectively. Here, the diode has a very low series inductance of 0.45 nH , parallel transition capacitance of 0.2 pF with $10\text{ k}\Omega$ resistance in OFF condition and 4Ω resistance in ON condition.

3. Simulated performance of triple band-notched UWB antenna

In this section, design procedure along with the parametric study of the UWB monopole antenna and triple-band notched UWB antenna is carried out in detail for providing a better understanding of its operation. As mentioned in Section 2, the design process begins with conceptualization of a reference rectangular printed monopole antenna for use in UWB systems. From Equation (1), it can also be concluded that the dimensions of the proposed monopole radiator affect the performance of the lower cut-off frequency of the antenna. However, the higher cut-off frequency and the impedance matching of the antenna are primarily contributed by the gap between the bottom-edge of the monopole radiator and top-edge of the ground plane (p_g). To examine this effect, a parametric analysis is conducted showing the variation of $|S_{11}|$ against frequency for different values of " L_g ". A change in the value of L_g also leads to a change in the value of " p_g ". As can be seen from Figure 3, the height of the ground plane has significant effect on improving the impedance

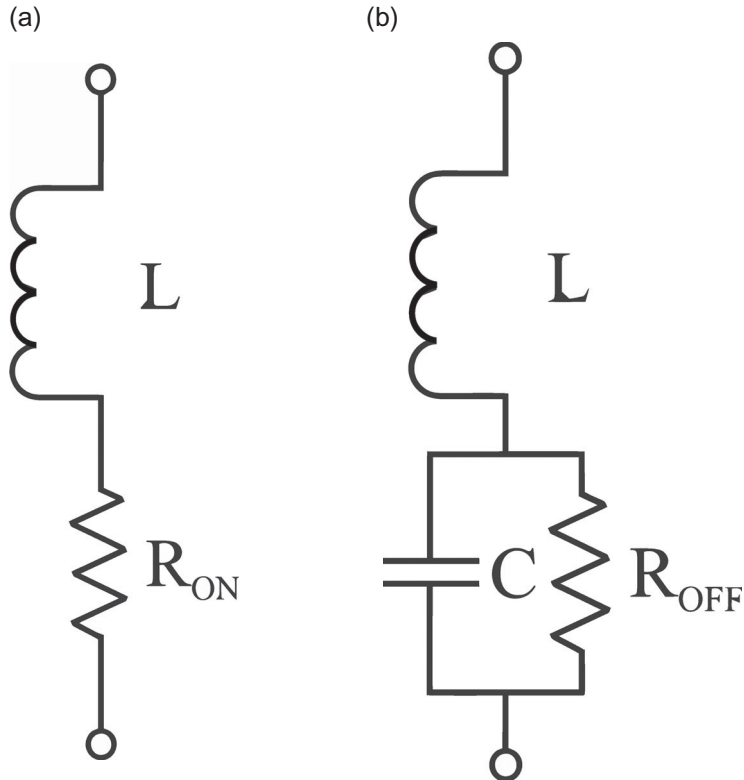


Figure 2. (a) Equivalent circuit model of PIN diode under ON condition. (b) Equivalent circuit model of PIN diode under OFF condition.

matching of the antenna. The ground plane serves as an impedance matching circuit and it tunes the input impedance and the operating bandwidth while the feed-gap is varied. The optimum value of “ L_g ” is therefore chosen to be equal to 15.1 mm.

Further, a parametric study is essential in order to understand the role of the three U-shaped slots in obtaining triple band-notch characteristics. To examine their effect, performance of the antenna embedded with the outer U-shaped slotted structure (Slot #1) is noted first (Figure 4(a)). Incorporation of Slot #1 on the radiating surface contributes in creating the first notched frequency (f_{n1}). The position of the notched frequency can be appropriately tuned by varying the total length of the U-shaped slot. The slot-width (W_1) is kept fixed at 0.6 mm. Further, Figure 4(a) illustrates that on increasing the value of L_1 , the notched frequency undergoes a downward shift from 3.28 to 2.62 GHz. The lower and higher cut-off frequencies remain unaffected. By incorporating the second U-shaped slot (Slot #2) on the radiating surface, a subsequent notched frequency (f_{n2}) is created. It is observed here that an increase in L_2 results in negative shift of the notch frequency from 3.95 GHz to 3.29 GHz as shown in Figure 4(b). Likewise, the third U-shaped slot (Slot #3) is etched on the radiator to realize one additional notch frequency (f_{n3}). Figure 4(c) plots the variation of simulated reflection coefficient against different values of slot-length L_3 . In this case also, it is observed that the notched frequency is a function

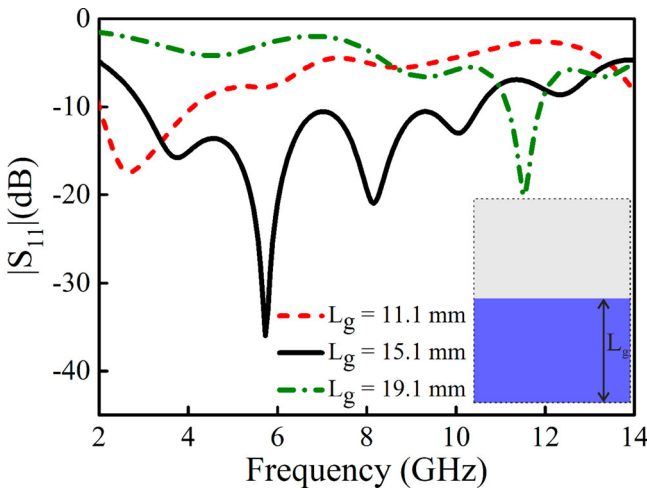


Figure 3. Simulated performance of reference UWB antenna for different values of L_g

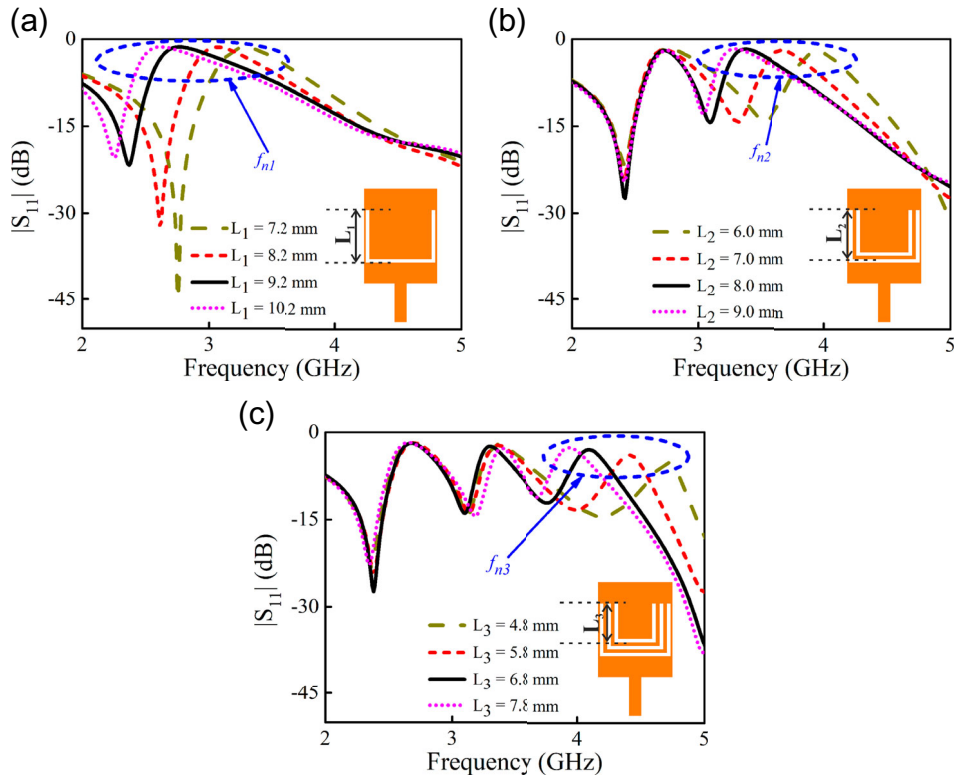


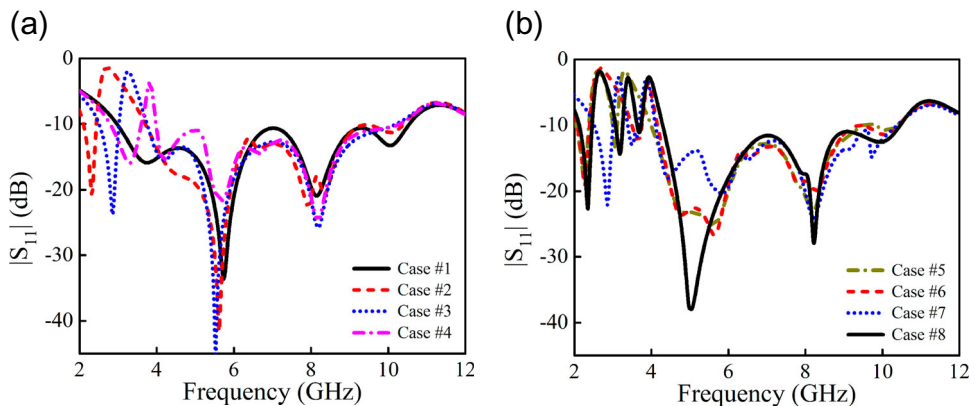
Figure 4. (a) Evolution of single-notch characteristics. (b) Evolution of dual-notch characteristics. (c) Evolution of triple-notch characteristics.

of the length of the U-shaped slot. Due to the compact size of the radiating patch, the U-shaped slots are implemented instead of a straight slot to ensure the quarter-wavelength characteristics.

Table 1. Different operating states of reconfigurable antenna.

OS	Diode state			Corresponding notched bands (GHz)					
	D ₁	D ₂	D ₃	f _{n1}	f _{n2}	f _{n3}	Notched Band-1	Notched Band-2	Notched Band-3
#1	ON	ON	ON	X	X	X	—	—	—
#2	OFF	ON	ON	✓	X	X	2.46–3.62	—	—
#3	ON	OFF	ON	X	✓	X	—	3.15–3.78	—
#4	ON	ON	OFF	X	X	✓	—	—	3.71–4.15
#5	OFF	OFF	ON	✓	✓	X	2.45–3.08	3.28–4.05	—
#6	OFF	ON	OFF	✓	X	✓	2.44–3.49	—	3.88–4.28
#7	ON	OFF	OFF	X	✓	✓	—	3.08–3.41	3.73–4.24
#8	OFF	OFF	OFF	✓	✓	✓	2.49–2.82	3.18–3.68	3.93–4.22

OS: Operating state.

**Figure 5.** (a) Simulated performance of reconfigurable antenna for different cases of operation from OS #1-OS #4. (b) Simulated performance of reconfigurable antenna for different cases of operation from OS #5-OS #8.

Further, as introduced in Section 2, reconfigurable characteristics with single, dual- and triple-band rejection capability are introduced by employing PIN diodes. By maintaining appropriate biasing conditions across the PIN diode, as described in Figure 1(c), eight switching operating states have been successfully realized. The diode D₁ is used to alter the outer U-slot effect to reconfigure the first notch frequency, while D₂ and D₃ is used to control the effect of middle and inner U-slot in order to reconfigure the second and third notch frequency, respectively. The different cases of switching conditions are listed in Table 1.

In Table 1, OS #1 represents the condition when all three diodes (D₁, D₂, and D₃) are maintained in forward bias condition. OS #2-OS #4 represents the conditions when forward bias condition is maintained across any two of the three PIN diodes. Similarly, when the forward bias voltage is applied across any one of the three diodes, the corresponding situations are named as OS #5, OS #6, and OS #7, respectively. Finally, OS #8 resembles the condition when all the diodes are maintained under reverse bias condition. Performance variation of $|S_{11}|$ against frequency, for antenna displayed in Figure 1(c), is plotted in Figure 5. The performance under conditions without notch and single-notched conditions is depicted in Figure 5(a), while the cases of dual- and triple-notched conditions are displayed in Figure 5(b).

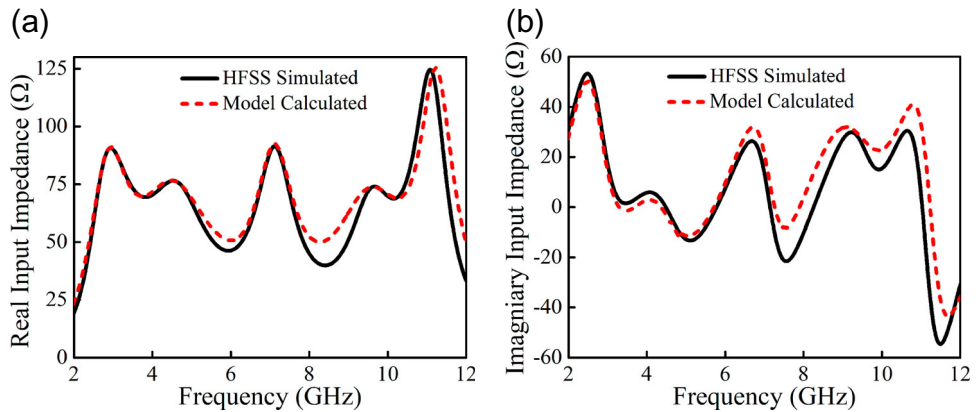


Figure 6. (a) Real input impedance comparison of reference UWB antenna. (b) Imaginary input impedance comparison of reference UWB antenna.

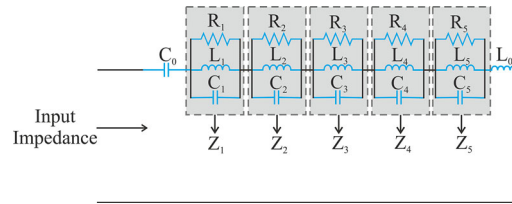


Figure 7. Equivalent circuit model for reference UWB antenna.

4. Derivation of equivalent circuit model

In this section, operating mechanism is further studied by deriving the lumped equivalent circuit models of the reference UWB antenna and triple band-notched UWB antenna, respectively. It is known fact about the UWB antenna that the large bandwidth is achieved due to the overlapping of several adjacent resonances and these resonances can be represented due to serially connected parallel R-L-C resonant circuits [34]. The modelling procedure begins with the determination of the resonant peaks from the simulated input impedance of reference UWB antenna. The equivalent parallel R-L-C resonant circuit model is then extracted from the simulated curve. The simulated real input impedance of the UWB antenna has five resonance peaks within the frequency span of 2–12 GHz as shown in Figure 6(a). Therefore the equivalent circuit of the reference antenna is constituted by connecting five parallel R-L-C resonant circuits in series as shown in Figure 7. Here two additional lumped components, L_0 and C_0 are also introduced to account for the impedance transformation due to probe inductance and the static antenna capacitance.

Based on the simulated variation of input impedance of the reference UWB antenna, the initial values for the parallel lumped R-L-C elements are determined using traditional resonance circuit theory [34] and it is mentioned using equation (6)–(8) as follows:

$$Q_i = \frac{f_i}{BW_i} \quad (6)$$

$$\omega_i = 2\pi f_i = \frac{1}{\sqrt{L_i C_i}} \quad (7)$$

$$Q_i = R_i \sqrt{\frac{C_i}{L_i}} = R_i C_i \omega_i \quad (8)$$

Here,

$i = 1, 2, 3, 4, 5$

Q_i = Quality factor of the i^{th} resonant circuit.

f_i = Resonant frequency of the i^{th} resonant circuit.

R_i = Real part of the impedance of the i^{th} resonant circuit.

C_i = Equivalent capacitance of the i^{th} resonant circuit.

L_i = Equivalent inductance of the i^{th} resonant circuit.

In order to determine the total input impedance of the equivalent circuit, the impedances of the individual stages are first calculated and then added together. The impedance value for the first parallel R-L-C resonant circuit can be determined as:

$$Z_1 = \frac{1}{\frac{1}{R_1} + \frac{1}{Z_{L1}} + \frac{1}{Z_{C1}}} = \frac{1}{\frac{1}{R_1} + \frac{1}{j\omega L_1} + j\omega C_1} \quad (9)$$

Now, Equation (9) can be re-arranged as:

$$Z_1 = \frac{R_1}{1 + jR_1 C_1 \omega_1 \left(\frac{\omega}{\omega_1} - \frac{1}{L_1 C_1 \omega_1 \omega} \right)} \quad (10)$$

For the first resonant circuit, the value for angular resonance frequency (ω_1) and Q-factor (Q_1) are obtained from Equations (7) and (8), respectively.

$$\omega_1 = 2\pi f_1 = \frac{1}{\sqrt{L_1 C_1}} \quad (11)$$

$$Q_1 = R_1 \sqrt{\frac{C_1}{L_1}} = R_1 C_1 \omega_1 \quad (12)$$

By replacing the value for ω_1 and Q_1 , in Equation (10), the overall expression for impedance of the first resonant circuit can be represented as:

$$Z_1 = \frac{R_1}{1 + jQ_1 \left(\frac{\omega}{\omega_1} - \frac{\omega_1}{\omega} \right)} \quad (13)$$

A similar procedure is followed to find out the impedance for the second, third, fourth and fifth parallel R-L-C resonant circuit (i.e. Z_2, Z_3, Z_4 and Z_5), respectively. The total input impedance of the UWB antenna can therefore be obtained as:

$$Z_{in,UWB}(\omega) = -\frac{j}{\omega C_0} + Z_1 + Z_2 + Z_3 + Z_4 + Z_5 + j\omega L_0 \quad (14)$$

$$Z_{in,UWB}(\omega) = j \left(\omega L_0 - \frac{1}{\omega C_0} \right) + \sum_{i=1}^n \frac{R_i}{1 + jQ_i \left(\frac{\omega}{\omega_i} - \frac{\omega_i}{\omega} \right)} \quad (15)$$

Table 2. Lumped element values of the equivalent circuit for reference UWB antenna.

Series LC		Resonant frequency (GHz)				
C ₀ (pF)	Lumped element	f ₁ = 2.94	f ₂ = 4.49	f ₃ = 7.10	f ₄ = 9.57	f ₅ = 11.22
1.06	R (ohm)	75.73	60.34	65.76	54.39	99.95
L ₀ (nH)	L (nH)	1.80	1.11	0.24	0.21	0.13
1.02	C (pF)	1.70	1.07	2.07	1.31	1.55

Thus, Equations (6)–(8) are utilized for calculating the initial values for the unknown lumped parameters (R_i, L_i and C_i) used in Figure 7. Based on the initially calculated values, the equivalent circuit is designed using commercially available software NI AWR Design Environment. Equations (9)–(15) are used to further optimize the value of lumped parameters based on curve-fitting approach by replacing the input impedance with values predicted from HFSS software. The optimized values of the unknown circuit elements are listed in Table 2. The impedance characteristics obtained from the circuit presented in Figure 7 are compared with the HFSS simulated input impedance and the corresponding comparison is plotted in Figure 6. It is observed here that the output of the proposed model is almost overlapping with corresponding full-wave simulated values.

By following a similar design procedure as done for reference UWB antenna, the circuit model of the triple band-notched UWB antenna is developed here. From the HFSS simulated impedances of the reference antenna (Figure 8), it is seen that at the first notched frequency band, the imaginary component crosses zero and changes from capacitive to inductive while the real component presents a low resistance, similar to the behaviour of a series RLC circuit, i.e. the corresponding band rejection structure (Slot #1) acts as a series RLC circuit. At the second notch frequency, the reactance is nearly crossing zero and has a negative derivative, whereas the resistance has a local maximum. It is a typical parallel-type resonance with large and rapid changes in the impedance values of both real and imaginary parts. A similar behaviour of the input impedance is observed at the third notch frequency. In this case, the corresponding equivalent circuit model is proposed, as shown in Figure 9, where one series and two additional parallel RLC resonator is incorporated to represent the triple-band notched structure. The total input impedance of this equivalent circuit can be determined by Equations (16)–(22), respectively.

From Figure 9, the total input impedance for the triple-notched UWB antenna can be determined as:

$$Z_{in,notch}(\omega) = \frac{Z_1(\omega)Z_2(\omega)}{Z_1(\omega) + Z_2(\omega)} \quad (16)$$

The impedance value for series R-L-C- resonance circuit, corresponding to the first notched frequency (f_{n1}) is determined as:

$$Z_1(\omega) = R_{n1} + Z_{Ln1} + Z_{Cn1} = R_{n1} + j\omega L_{n1} - j\frac{1}{\omega C_{n1}} \quad (17)$$

$$Z_1(\omega) = R_{n1} \left[1 + j \left(\omega \frac{L_{n1}}{R_{n1}} - \frac{1}{\omega C_{n1} R_{n1}} \right) \right] \quad (18)$$

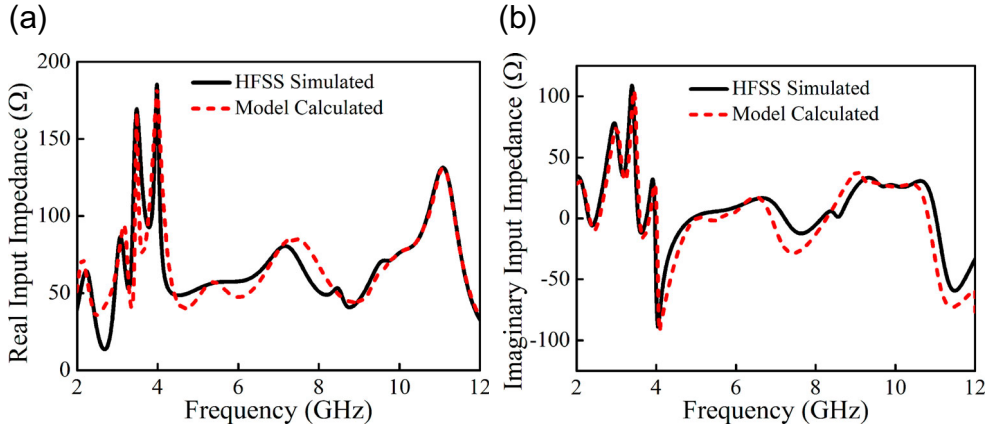


Figure 8. (a) Real input impedance comparison of notched antenna. (b) Imaginary input impedance comparison of notched antenna.

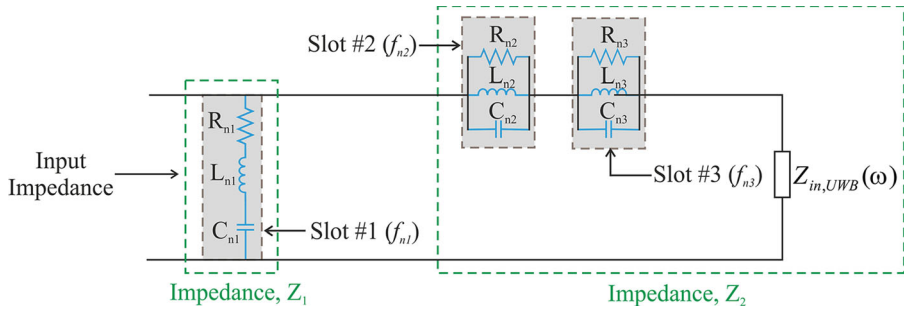


Figure 9. Equivalent circuit model for triple-notched UWB antenna.

For the series resonant circuit, the value for angular resonance frequency (ω_{n1}) and Q-factor (Q_{n1}) can be computed from Equations (19) and (20), as mentioned below:

$$\omega_{n1} = 2\pi f_{n1} = \frac{1}{\sqrt{L_{n1}C_{n1}}} \quad (19)$$

$$Q_{n1} = \frac{1}{R_{n1}} \sqrt{\frac{L_{n1}}{C_{n1}}} = \frac{1}{R_{n1}C_{n1}\omega_{n1}} \quad (20)$$

By substituting the values of ω_{n1} and Q_{n1} , in Equation (18) and then re-arranging the terms, the impedance value is obtained as:

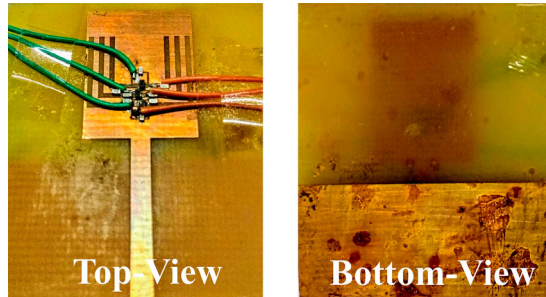
$$Z_1(\omega) = R_{n1} \left(1 + jQ_{n1} \left(\frac{\omega}{\omega_{n1}} - \frac{\omega_{n1}}{\omega} \right) \right) \quad (21)$$

Further, the impedances of the two parallel R-L-C resonant circuits can be derived by modifying Equation (13). The total impedance $Z_2(\omega)$ of cascaded parallel R-L-C network can thus be represented as:

$$Z_2(\omega) = \frac{R_{n2}}{1 + jQ_{n2} \left(\frac{w}{w_{n2}} - \frac{w_{n2}}{w} \right)} + \frac{R_{n3}}{1 + jQ_{n3} \left(\frac{w}{w_{n3}} - \frac{w_{n3}}{w} \right)} + Z_{in}(\omega) \quad (22)$$

**Table 3.** Equivalent circuit model values for Antenna #2.

Lumped element	Notched frequency (GHz)		
	$f_{n1} = 2.47$	$f_{n2} = 3.09$	$f_{n3} = 3.73$
R (ohm)	82.89	239.9	123.6
L (nH)	3.29	0.45	0.40
C (pF)	1.90	4.48	4.16

**Figure 10.** Fabricated image of proposed reconfigurable antenna.

In this case, also, the initial values of the lumped parameters are determined from Equations (19)–(20) for Slot #1. Similarly, for Slot #2 and Slot #3, Equations (6)–(8) are utilized to make the initial approximation of the unknown R-L-C elements. Next, by applying curve-fitting approach on Equations (16)–(22), optimized value for the unknown parameters of the triple band-notched equivalent circuit is computed. For the first notched frequency (f_{n1}), the equivalent values of the series R-L-C parameters are obtained as: $R_{n1} = 82.89 \Omega$, $L_{n1} = 3.29 \text{ nH}$, and $C_{n1} = 1.90 \text{ pF}$. Similarly, for the second notched-frequency (f_{n2}), the values of parallel R-L-C circuit is noted as: $R_{n2} = 239.9 \Omega$, $L_{n2} = 0.45 \text{ nH}$, and $C_{n2} = 4.48 \text{ pF}$. Finally, for third notched-frequency (f_{n3}), $R_{n3} = 123.6 \Omega$, $L_{n3} = 0.40 \text{ nH}$, and $C_{n3} = 4.16 \text{ pF}$, are the optimum values calculated for the parallel R-L-C circuit. Further, the optimized values of the unknown resistors (R_{n1}, R_{n2}, R_{n3}), inductors (L_{n1}, L_{n2}, L_{n3}), and capacitors (C_{n1}, C_{n2}, C_{n3}) are listed in Table 3. Figure 8 further compares the input impedance simulated by HFSS to the calculated one by the equivalent circuit model.

5. Experimental validation

The compact configuration of reconfigurable triple notched antenna, illustrated in Figure 1(c), has been fabricated and characterized in order to justify the achievability of the suggested layout. A snapshot of the fabricated prototype displaying top- and bottom-view is presented in Figure 10. Agilent E8362B vector network analyzer (VNA) and an automatic anechoic chamber have been used for measuring different performance parameters of the prototype. The antenna model is implemented using low-cost FR4 epoxy substrate ($\epsilon_r = 4.4$, and loss tangent = 0.02 and thickness $h = 1.6 \text{ mm}$). Overall dimension of the antenna is optimized to $31.3 \times 34.9 \times 1.6 \text{ mm}^3$. The simulation analysis of the proposed geometry is executed using HFSS v14.0 software [35].

To demonstrate the validity of the simulation and circuit analysis, the simulated performance of the reflection coefficient obtained from HFSS and AWR software is compared

to that of the experimental data. From the Figure 11, it can be argued that the variation of reflection coefficient agrees reasonably well over the entire operating frequency range.

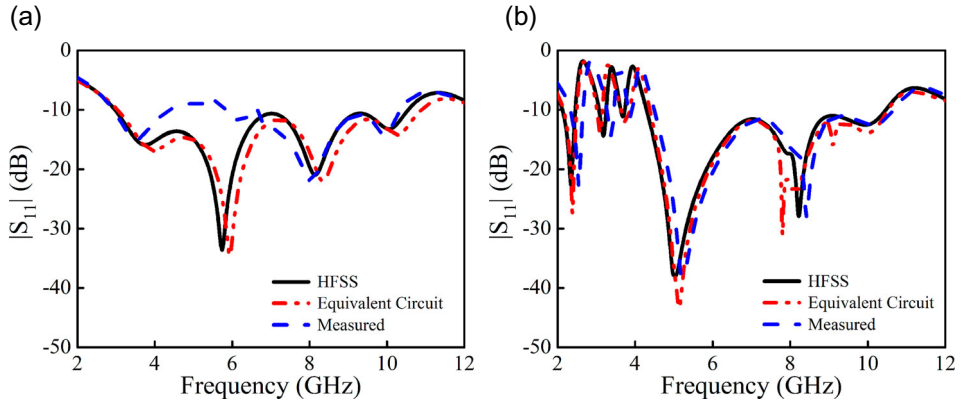


Figure 11. (a) Simulated and measured performance comparison of reconfigurable antenna for UWB operating state (OS #1). (b) Simulated and measured performance comparison of reconfigurable antenna for triple-notched operating state (OS #8).

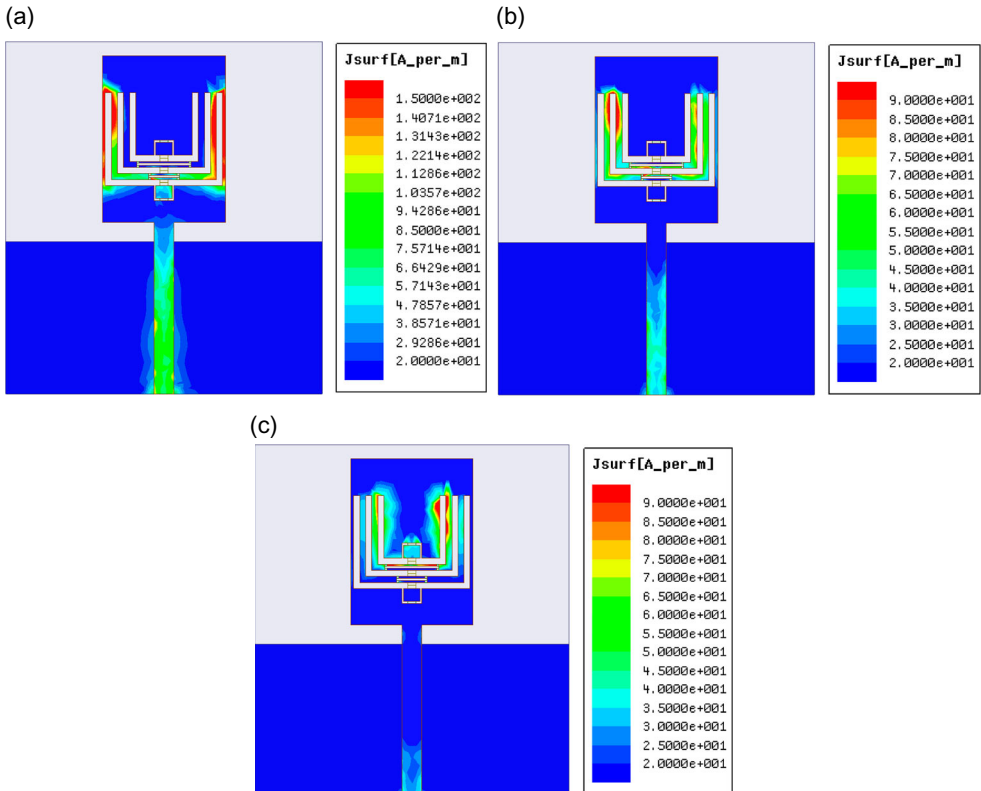


Figure 12. (a) Surface current distribution for reconfigurable antenna at 2.69 GHz. (b) Surface current distribution for reconfigurable antenna at 3.31 GHz. (c) Surface current distribution for reconfigurable antenna at 4.15 GHz.

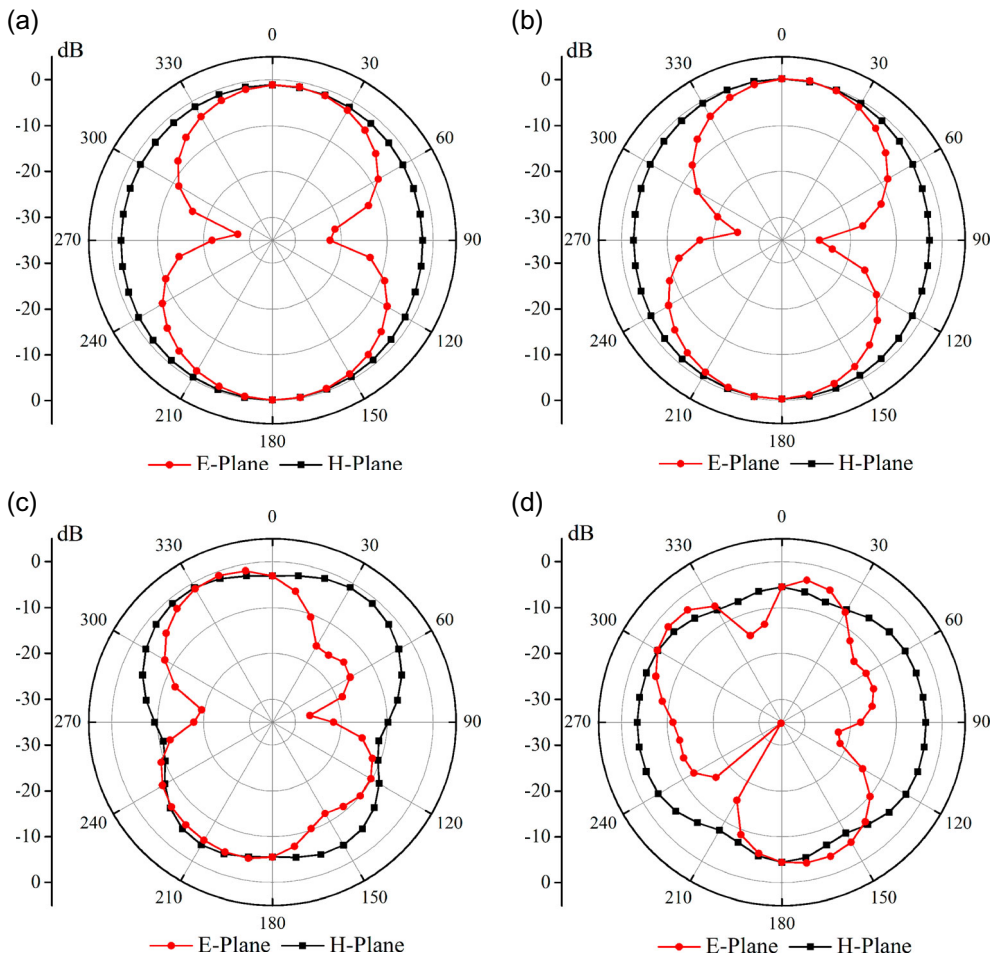


Figure 13. (a) Realized Radiation pattern of reconfigurable antenna at 3.68 GHz. (b) Realized Radiation pattern of reconfigurable antenna at 5.75 GHz. (c) Realized Radiation pattern of reconfigurable antenna at 8.14 GHz. (d) Realized Radiation pattern of reconfigurable antenna at 10.12 GHz.

In order to understand the operating principle behind the realization of the notched band phenomenon, the simulated current distribution of reconfigurable antenna, introduced in Figure 1(c), is plotted in Figure 12. At the notch frequency surface current is found to be concentrated at the respective U-shaped slots.

Next, the normalized measured radiation performance in the two principal E- and H-planes, for the reconfigurable antenna is depicted in Figure 13. The radiation patterns are obtained at the resonance frequencies, with the antenna being operated in the UWB state (OS #1). Figure 13 illustrates that the antenna exhibits a stable radiation pattern in lower frequency band like a traditional monopole with omnidirectional radiation pattern in the H-plane and bi-directional radiation pattern in the E-plane. However, at higher frequency band irregularities in the radiation patterns are observed which is contributed by the hybrid mode of standing and travelling waves. Further, in Figure 14, measured gain of the antenna

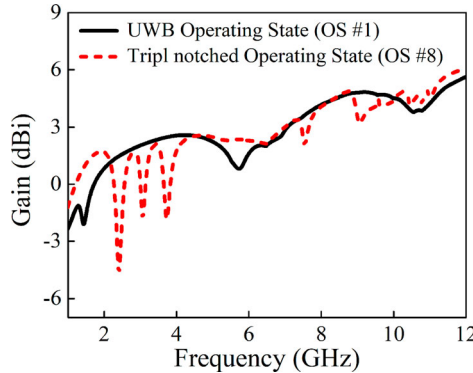


Figure 14. Measured gain response of reconfigurable antenna (OS #1 and OS #8).

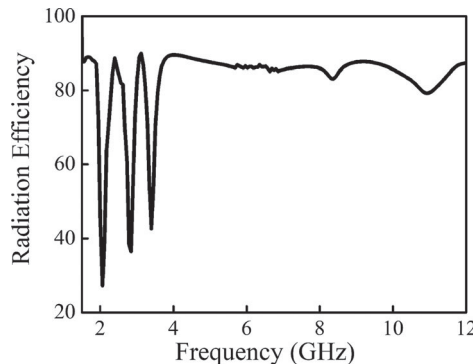


Figure 15. Radiation efficiency of reconfigurable triple band-notched antenna (OS #8).

at UWB (OS #1) and triple-band notched (OS #8) states of operation are plotted. The variation of gain is more than 2 dBi in both the states of operation. However, a sharp decrease in gain value is observed at the three notched frequencies, which establishes the simultaneous rejection of interferences from the C-band satellite and WiMAX systems. Similarly, the simulated radiation efficiency is plotted in Figure 15 for the triple notched operating state (OS #8) of the antenna. The radiation efficiency is between 80 and 90% over the operating bandwidth but drops below 45% at all three notched frequencies.

Finally, the performance of the proposed antenna has been compared with some recently published configurations on band-notched UWB antennas. Table 4 lists the comparison with existing literature in terms of antenna dimensions, and number of notches obtained along with the notched frequency bands. Additionally, the number of reconfigurable states obtained in the case of the proposed structures with the number of active devices used to accomplish these operating states has also been noted down. It can be inferred that the antenna design introduced in this work is comparable with the existing configurations in terms of the size. Besides, the unique feature of this work can be pointed out as the successful realization of eight different reconfigurable states by means of only three PIN diode switches.

**Table 4.** Performance comparisons with existing literatures.

Ref.	Dimension (mm ²)	Notch generation technique	No. of notches	Notched bands (GHz)	Reconfigurable states	Switches used
[23]	20 × 20	Π-shaped Slot	1	5.03–5.94	2	1
[24]	22 × 29	F-shaped parasitic element	1	4.9–5.7	2	1
[25]	27.5 × 8	G-shaped radiator	1	3.5–4.95	2	1
[26]	20 × 20	Inverted U-shaped slots	2	3.15–3.85, 5.43–6.1	4	2
[27]	45 × 40	T-shaped stub, Semi circular parasitic strip	2	3.7–4.2, 5.15–5.825	4	3
[28]	28 × 28	H-shaped slot C-shaped arms, L-shaped slots	3	3.20–3.75, 5.05–5.90, 8–8.45	5	2
[29]	24.5 × 20	C-shaped slots, Split-ring resonator	3	3.2–4.1, 5.1–5.9, 7.7–8.6	4	2
[30]	25 × 21	C-shaped slot, L-shaped slots, Split-ring resonator	3	N. A.	4	2
This Work	34.9 × 31.3	U-shaped slots	3	2.16–2.41, 2.51–2.89, 3.13–3.84	8	3

N. A.: Not available.

6. Conclusions

In this paper, a triple band-notched UWB antenna, which has the ability to reconfigure its notched characteristics, is proposed. The antenna exhibits wide impedance matching and can be implemented in UWB systems. Three U-shaped slots in the radiating patch are used to reject three frequency bands operating at 2.68, 3.31, and 4.15 GHz, respectively. Further, to enhance the versatility of the proposed antenna, reconfigurable property has been introduced. By turning appropriate switches ON or OFF, desirable state of operation can be easily achieved. In authors' knowledge, design and validation of reconfigurable antenna for eight different cases have rarely been achieved in the open literature. The proposed configurations have the advantages of simple structure, easy design procedure, low profile, low cost, reconfigurable functionality, and ultra-wide operating band.

Acknowledgements

This work was supported by the Science and Engineering Research Board (SERB), Department of Science and Technology (DST), Govt. of India (GoI) under a research grant No: SB/S3/EECE/093/2016.

Disclosure statement

No potential conflict of interest was reported by the authors.

Funding

This work was supported by Science and Engineering Research Board [Research grant No: SB/S3/EECE/093/2016].

Notes on contributors

Partha Pratim Shome received his BTech Degree in the stream of Electronics and Communication Engineering and MTech Degree with specialisation in Communication System Engineering both from KIIT University, Bhubaneswar. At present, he is working as a full-time PhD Scholar at the National Institute of Technology Silchar, India. His current research interests include Band-notched Antennas, Reconfigurable Antennas, Ultra-wideband Filters, Printed Filtennas and Neural Networks. He is an active student member of IEEE APS and MTT (USA).

Taimoor Khan is presently an Assistant Professor in the Department of Electronics and Communication Engineering at the National Institute of Technology Silchar, India where he serves as a full-time faculty member since 2014. Prior to joining NIT Silchar, he served several organizations like: Delhi Technological University (Formerly Delhi College of Engineering), Govt. of NCT of Delhi, Delhi, India as an Assistant Professor for more than two years; Netaji Subhas Institute of Technology Patna, India as an Associate Professor and Head of the Department for one and half year and Shobhit Institute of Engineering and Technology, Meerut, Uttar Pradesh, India as a Lab Instructor, Lecturer and Assistant Professor for more than nine years. Dr Khan awarded his PhD Degree in Electronics and Communication Engineering from National Institute of Technology Patna, India in the year 2014. He obtained his Master Degree in Communication Engineering from Shobhit Institute of Engineering and Technology (A Deemed to be University), Meerut, Uttar Pradesh, India in 2009, Bachelor Degree in Electronics and Communication Engineering from The Institution of Engineers (India), Kolkata, India in the year 2005 and Polytechnic Diploma in Electronics Engineering from Government Polytechnic Saharanpur, Uttar Pradesh, India in 2001. His active research interest includes Printed Microwave Circuits, Electromagnetic Bandgap Structures, Dielectric Resonator and its Applications and Computational Intelligence Paradigms in Electromagnetics. He has published over 70 research papers in international journals and conference proceedings of repute. Dr Khan is involved in executing four sponsored projects funded by Govt. of India and is also a member of the Editorial Board of RFMiCAE Journal. He is an active Senior Member IEEE, Fellow, IETE, Senior Member, URSI.

References

- [1] Kshetrimayum RS. An introduction to UWB communication systems. *IEEE Potentials*. 2009; 28:9–13.
- [2] Federal Communications Commission. First report and order: revision of Part 15 of the commission's rules regarding ultra-wideband transmission system . Washington (DC): FCC; 2002. p. 98–153.
- [3] Shome PP, Khan T, Laskar RH. CSRR-loaded UWB monopole antenna with electronically tunable triple band-notch characteristics for cognitive radio applications. *Microw Opt Technol Lett*. 2020;62(9):2919–2929.
- [4] Doddipalli S, Kothari A. Compact UWB antenna with integrated triple notch bands for WBAN applications. *IEEE Access*. 2018;7:183–190.
- [5] Ojaroudi M, Ghanbari G, Ojaroudi N, et al. Small square monopole antenna for UWB applications with variable frequency band-notch function. *IEEE Antennas Wirel Propag Lett*. 2009;8:1061–1064.
- [6] Dong YD, Hong W, Kuai ZQ, et al. Analysis of planar ultrawideband antennas with on-ground slot band-notch structures. *IEEE Trans Antennas Propag*. 2009;57:1886–1893.
- [7] Xie M, Guo Q, Wu Y. Design of a miniaturized UWB antenna with band-notched and high frequency rejection capability. *J Electromagn Waves Appl*. 2012;25(8–9):1103–1112.
- [8] Moghadasi MN, Sadeghzadeh RA, Sedghi T, et al. UWB CPW-fed fractal patch antenna with band-notched function employing folded T-shaped element. *IEEE Antennas Wirel Propag Lett*. 2013;12:504–507.

- [9] Peng L, Wen BJ, Li XF, et al. CPW fed UWB antenna by EBGs with wide rectangular notched-band. *IEEE Access*. 2016;4:9545–9552.
- [10] Azim R, Islam MT, Mobashsher AT. Dual band-notch UWB antenna with single tri-arm resonator. *IEEE Antennas Wirel Propag Lett*. 2014;13:670–673.
- [11] Siddiqui JY, Saha C, Antar YMM. Compact SRR loaded UWB circular monopole antenna with frequency notch characteristics. *IEEE Trans Antennas Propag*. 2014;62(8):4015–4020.
- [12] Mehdipour A, Parsa A, Sebak AR, et al. Miniaturised coplanar waveguide-fed antenna and band-notched design for ultra-wideband applications. *IET Microw, Antennas Propag*. 2009;3(6):974–986.
- [13] Nouri A, Dadashzadeh GR. A compact UWB band-notched printed monopole antenna with defected ground structure. *IEEE Antennas Wirel Propag Lett*. 2011;10:1178–1181.
- [14] Li T, Zhai HQ, Zhu C, et al. Design and analysis of compact printed dual band-notched ultrawideband (UWB) antenna. *J Electromagn Waves Appl*. 2013;27(5):560–571.
- [15] Safia OA, Nedil M, Talbi L, et al. Coplanar waveguide-fed rose-curve shape UWB monopole antenna with dual-notch characteristics. *IET Microw, Antennas Propag*. 2018;12(7):1112–1119.
- [16] Sarkar D, Srivastava KV, Saurav K. A compact microstrip-fed triple band-notched UWB monopole antenna. *IEEE Antennas Wirel Propag Lett*. 2014;13:396–399.
- [17] Ghosh A, Mandal T, Das S. Design and analysis of triple notch ultrawideband antenna using single slotted electromagnetic bandgap inspired structures. *J Electromagn Waves Appl*. 2019;33(11):1391–1405.
- [18] Sung Y. Quad band-notched ultrawideband antenna with a modified H-shaped resonator. *IET Microw, Antennas Propag*. 2013;7(12):999–1004.
- [19] Chakraborty M, Pal S, Chattoraj N. Quad notch UWB antenna using combination of slots and split ring resonators. *Int J RF Microw Comput Aided Eng*. 2019;30(3):1–10.
- [20] Rahman M, Khan W T, Imran M. Penta-notched UWB antenna with sharp frequency edge selectivity using combination of SRR, CSRR, and DGS. *AEU-Int J Electron Commun*. 2018;93:116–122.
- [21] Modak S, Khan T, Laskar RH. Penta-band notched ultra-wideband monopole antenna loaded with electromagnetic bandgap-structures and modified U-shaped slots. *Int J RF Microw Comput Aided Eng*. 2019;29(12):1–11.
- [22] Haupt RL, Lanagan M. Reconfigurable antennas. *IEEE Antennas Propag Mag*. 2013;55(1):49–61.
- [23] Valizade A, Ghobadi C, Nourinia J, et al. A novel design of reconfigurable slot antenna with switchable band notch and multi resonance functions for UWB applications. *IEEE Antennas Wirel Propag Lett*. 2012;11:1166–1169.
- [24] Yadav D, Abegaonkar MP, Koul SK, et al. A novel frequency reconfigurable monopole antenna with switchable characteristics between band-notched UWB and WLAN applications. *Prog Electromagn Res C*. 2017;77:145–153.
- [25] Toktas A, Yerlikaya M. A compact reconfigurable ultra-wideband G-shaped printed antenna with band-notched characteristics. *Microw Opt Technol Lett*. 2019;61(1):245–250.
- [26] Badamchi B, Nourinia J, Ghobadi C, et al. Design of compact reconfigurable ultra-wideband slot antenna with switchable single/dual band notch functions. *IET Microwave, Antennas Propag*. 2014;8(8):541–548.
- [27] Kalteh AA, Zadeh GRD, Moghadasi MN, et al. Ultra-wideband circular slot antenna with reconfigurable notch band function. *IET Microw, Antennas Propag*. 2012;6:108–112.
- [28] Nasrabadi E, Rezaei P. A novel design of reconfigurable monopole antenna with switchable triple band-rejection for UWB applications. *Int J Microw Wirel Technol*. 2015;8(8):1223–1229.
- [29] Tripathi S, Mohan A, Yadav S. A compact fractal UWB antenna with reconfigurable band-notch functions. *Microw Opt Technol Lett*. 2016;58(3):509–514.
- [30] Nazeri AH, Falahati A, Edwards RM. A novel compact fractal UWB antenna with triple reconfigurable notch reject bands applications. *AEU-Int J Electron Commun*. 2019;101:1–8.
- [31] Shome PP, Khan T, Laskar RH. A state-of-art review on band-notch characteristics in UWB antennas. *Int J RF Microw Comput Aided Eng*. 2018;29:1–16.
- [32] Ray KP. Design aspects of printed monopole antennas for ultra-wide band applications. *Int J Antennas Propag*. 2008;2008:8.

- [33] Sanyal R, Sarkar PP, Chowdhury SK. Quasi-self-complementary ultra-wideband antenna with band rejection characteristic. *Int J Microw Wirel Technol.* **2018**;10(03):336–344.
- [34] Pele I, Chousseaud A, Toutain S. Simultaneous modelling of impedance and radiation pattern antenna for UWB pulse modulation. *IEEE APS International Symposium Digest*; 2004 Jun 20–25; Monterey, CA: IEEE; 2004.
- [35] HFSS v14.0.